

Low-Threshold Epitaxially Grown 1.3- μm InAs Quantum Dot Lasers on Patterned (001) Si

Chen Shang , Yating Wan , Justin C. Norman , *Member, IEEE*, Noelle Collins, Ian MacFarlane, Mario Dumont, Songtao Liu, Qiang Li, *Member, IEEE*, Kei M. Lau , *Fellow, IEEE*, Arthur C. Gossard, *Life Fellow, IEEE*, and John E. Bowers , *Fellow, IEEE*

Abstract—A three-fold reduction of threshold current, with a minimum threshold current density of 286 A/cm², a maximum operating temperature of 80 °C, and a maximum 3-dB bandwidth of 5.8 GHz was achieved for 1.3- μm InAs quantum dot lasers on patterned, on-axis (001) Si. This was enabled by the reduced threading dislocation density (from 7×10^7 to 3×10^6 cm⁻²), and optimized probe design. The patterned Si produced antiphase domain free material in the coalesced GaAs buffer layer with reduced misfit/threading dislocation nucleation, without the use of Ge/GaP buffers or substrate miscut. Utilizing aspect ratio trapping, cyclic thermal annealing, and dislocation filter layers, high-quality III-V on Si devices were grown, demonstrating the compelling advantages of this patterned Si template for a monolithic Si photonics integration platform.

Index Terms—Integrated optoelectronics, quantum dots, wafer, scale integration.

I. INTRODUCTION

THE explosive growth of Internet Protocol (IP) traffic is driving data centers into the Zettabyte Era. Consuming 1.5% of the total energy consumed in the U.S. at a cost of \$4.5B, the data centers' energy consumption is predicted to triple by 2020 [1]. Today, Si photonics supplies 100% of the 80 km dense wavelength division multiplexing (DWDM), >75% of the parallel single mode 4-channel (PSM4), and >50% of the

Manuscript received January 31, 2019; revised April 29, 2019; accepted June 28, 2019. Date of publication July 9, 2019; date of current version July 23, 2019. This work was supported in part by Advanced Research Projects Agency-Energy (16212115), in part by the American Institute for Manufacturing—Integrated Photonics (DE-AR0000672), in part by the Research Grants Council of Hong Kong, and in part by the Innovation Technology Fund of Hong Kong (ITS/320/14). (Chen Shang, Yating Wan, and Justin C. Norman contributed equally to this work.) (Corresponding author: Yating Wan.)

C. Shang, J. C. Norman, and A. C. Gossard are with Materials Department, University of California, Santa Barbara, Santa Barbara, CA 93106 USA (e-mail: shang00@umail.ucsb.edu; jnorman@ucsb.edu; acgossard@gmail.com).

Y. Wan, S. Liu, and J. E. Bowers are with the Institute for Energy Efficiency, University of California, Santa Barbara, Santa Barbara, CA 93106 USA (e-mail: yatingwan@ucsb.edu; stliu@ece.ucsb.edu; bowers@ece.ucsb.edu).

N. Collins, I. MacFarlane, and M. Dumont are with the Department of Electrical and Computer Engineering, University of California, Santa Barbara, Santa Barbara, CA 93106 USA (e-mail: noellecollins@ucsb.edu; ian@macfarlanehome.com; mariodumont@ucsb.edu).

Q. Li and K. M. Lau are with the Department of Electronic and Computer Engineering, The Hong Kong University of Science and Technology, Hong Kong (e-mail: qli@connect.ust.hk; eekmlau@ust.hk).

Color versions of one or more of the figures in this paper are available online at <http://ieeexplore.ieee.org>.

Digital Object Identifier 10.1109/JSTQE.2019.2927581

2 km coarse 4×25 Gbps coarse wavelength division multiplexing (CWDM4) for Microsoft [2]. This technology is currently fueling high bandwidth density interconnection links and is primed to serve other growth markets such as light detection and ranging (LIDAR) and chip-scale wearable sensors [3]. Although Si-based light guiding, modulation and detection technologies have been explored extensively with impressive achievements [4], the indirect bandgap has hampered the development of an on-chip light source.

Recently, InAs quantum dots (QDs) have demonstrated themselves as the most promising candidate for achieving high performance light emitters epitaxially grown on Si [5]–[12]. The effective carrier localization in QDs considerably improves laser reliability over quantum well (QW) lasers on Si by suppressing growth of 110 dark-line defects [14]. The extrapolated mean time to failure, as defined by doubling of the initial threshold current, are now more than 10, 000, 000 hours for state-of-art QD lasers on Si at 35 °C [15]. In contrast, the most prolonged lifetime reported among GaAs-based QW lasers on Si is merely ~ 200 h after more than a decade of research [16].

To date, intensive research has been conducted to migrate this field to the use of complementary metal–oxide–semiconductor (CMOS) compatible on-axis Si substrates [17]–[21]. Various novel methods have been applied to solve the anti-phase domain (APD) problem, obviating the need for miscut substrates. These approaches range from direct nucleation of a GaAs film with special Si wafer preparation [17], [18], growing an Al_{0.3}Ga_{0.7}As seed layer [19], the use of a thin GaP buffer layer [15], 0.15° misorientation in the [110] direction [20], U-shaped patterned Si (001) substrates to obtain (111)-faceted-sawtooth Si hollow structures [21], and patterned growth on exposed {111} V-groove facets of silicon [22]. Leveraging the aspect ratio trapping effects, we previously demonstrated electrically injected QD lasers grown on on-axis (001) Si with {111} V-groove facets [23]. The “tiara”-like structures formed by the patterned Si simultaneously circumvent the issue of APDs and effectively filter out stacking faults in the coalesced GaAs buffer layer without additional Ge/GaP buffers or substrate miscut [24]. A comprehensive comparison of the lasing characteristics in devices with the same active structure and geometry but fabricated on this V-groove Si template in conjunction with our simultaneously developed GaP/Si template has been made [25]. Despite the fact that the GaP/Si possesses three-fold lower defect densities, devices on V-groove Si substrate achieved continuous-wave

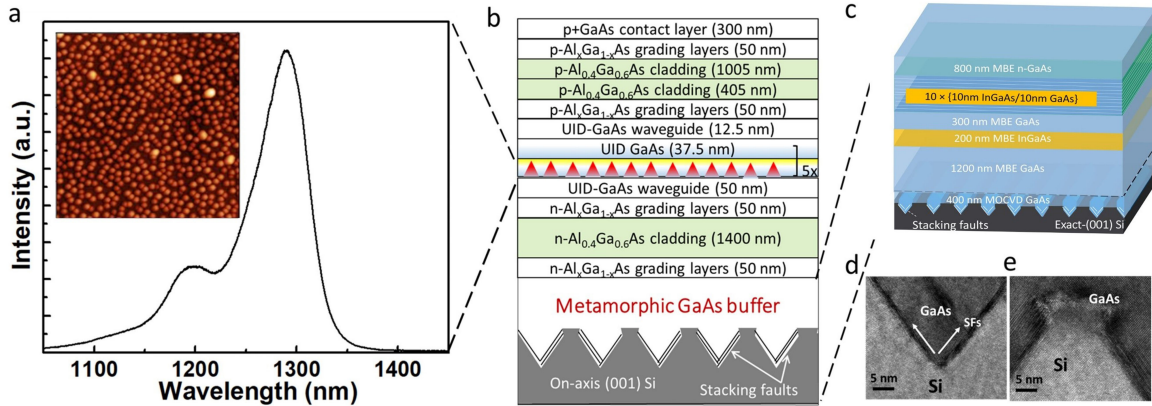


Fig. 1. (a) Photoluminescence spectrum of the as-grown sample. Inset: atomic force microscopy image of QD with a density of $6.4 \times 10^{10} \text{ cm}^{-2}$. The image has a size of $1 \times 1 \mu\text{m}^2$. (b) The full stack of the laser structure. (c) Schematic image of the buffer structure. Materials above the dashed line are grown by MBE. (d) and (e) Cross-sectional TEM images of the V-grooved structure, showing stacking faults (indicated by the white arrows) trapped by the Si pockets.

(CW) lasing with thresholds as low as 36 mA for a $6 \times 1200 \mu\text{m}^2$ ridge laser with 95% reflectivity coating on one facet [23] and submilliwatt threshold of 0.6 mA for a microring laser with an outer radius of $5 \mu\text{m}$ and a ring width of $3 \mu\text{m}$ [12]. Furthermore, the V-groove Si is advantageous in providing a smoother surface and thinner buffer layers which saves growth time, and is beneficial for subsequent device fabrication [26].

Here, by combining the additional effects of thermal cyclic annealing and strained-layer superlattices, a record-low threading dislocation density (TDD) of $3 \times 10^6 \text{ cm}^{-2}$ on a V-groove Si template was achieved. This is more than a 20-fold reduction over the previously reported TDD on V-groove Si [22], half of the value in the state-of-art GaP/Si template [10], and closes the gap relative to the best reported dislocation densities for lasers on Si [7], [20]. The significant decrement of TDD translates into a three-fold reduction of threshold currents (minimum value of 12 mA here, while the value is 36 mA in [22]), with a minimum threshold current density of 286 A/cm^2 , and a maximum operating temperature of 80°C . Furthermore, by optimizing the probe design, a maximum 3 dB bandwidth of 5.8 GHz was achieved. This is larger than the theoretically predicted modulation bandwidth maximum (of 5 GHz) in a recent report of monolithic $1.3 \mu\text{m}$ InAs/GaAs QD lasers on Si [27].

II. EXPERIMENTAL PROCEDURE

The GaAs-on-v-groove Si template, shown in Fig. 1(c), was grown by the combined effort of both metal-organic chemical vapor deposition [23] (the first 400 nm coalesced GaAs) and solid-source molecular beam epitaxy (MBE). The GaAs nanowires were first selectively grown in the V-grooves, with openings of 70 nm, of the patterned (001) Si wafer on {111} planes. The SiO_2 stripes were then removed using buffered oxide etch (BOE). The GaAs nanowires coalesced into a continuous thin film after growing to a total thickness of 100 nm at 600°C . Then, 300 nm of additional GaAs was deposited for planarization. Stacking faults nucleated at the GaAs-Si interface accommodate for the 4.1% lattice mismatch, which were then blocked by the Si ridges and thereby contained in the V-grooves.

The high index growth plane ensured that no APDs would form at the interface. It is worth mentioning that there is more than one strain relaxation mechanism for V-groove epitaxy under different growth parameters [28]. The result from IMEC [29] shows the relaxation of III/V on {111} facets based on misfit and TD formation.

Here, by making use of a different strain relaxation mechanism (compared to blanket epitaxy in [16]–[18]) based on a highly twinned region with thickness $< 10 \text{ nm}$, the tip of the Si ridges ensures the stress-relaxing layer is confined within the V-shaped trenches. This phenomenon is shown in the cross-section bright-field transmission electron microscopy (TEM) image in Fig. 1(d) and (e). Thus, the V-groove approach eliminates APDs and moderately reduces TDD, while the main defect reduction was realized through the remaining structure of the GaAs-on-Si buffer by MBE [22]. In the MBE buffer, four cycles of temperature annealing from 400°C to 700°C were applied after the initial 1200 nm GaAs growth, which provides additional kinetic energy for the TDs to increase their in-plane movement and promotes them to meet and annihilate. Next, 200 nm of $\text{In}_{0.1}\text{Ga}_{0.9}\text{As}$ and ten periods of $\text{In}_{0.1}\text{Ga}_{0.9}\text{As}/\text{GaAs}$ (10 nm/10 nm) superlattices were employed to promote lateral movement of the TDs through the induced compressive stress. The buffer structure was finished with 800 nm *n*-doped GaAs with a concentration of $2 \times 10^{18} \text{ cm}^{-3}$. A root-mean-square roughness of $\sim 2.8 \text{ nm}$ was obtained across a scanning area of $5 \times 5 \mu\text{m}^2$ in the atomic force microscopy (AFM) image, shown in Fig. 2(a). The final TDD was measured to be $3 \times 10^6 \text{ cm}^{-2}$ by electron channeling contrast imaging (ECCI) shown in Fig. 2(b).

The full laser structure with 5 layers of QD as the active region was grown on top of the buffer structure, as shown in Fig. 1(b). A GaAs/AlGaAs graded-index separate confinement heterostructure was used as the cladding layer for both optical and electrical confinement. Fig. 1(a) shows the room temperature photoluminescence (PL) spectrum of the InAs QDs, which has a peak intensity around 1290 nm for the ground-state transition and a full width at half maximum of about 30 meV. The nominal InAs thickness was 2.75 ML. The optimized growth temperature was 495°C under As_4 overpressure at a V/III of 35.

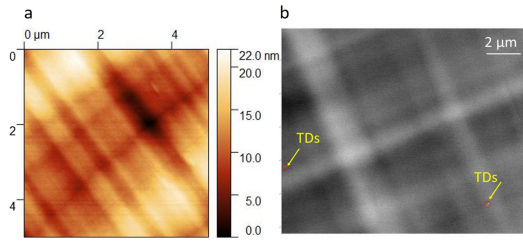


Fig. 2. (a) AFM and (b) ECCI of the buffer structure. In the AFM, a root-mean-square roughness of ~ 2.7 nm was obtained across a scanning area of $5 \times 5 \mu\text{m}^2$. The vertical bar is 22 nm. In the ECCI, TDD is as low as $3 \times 10^6 \text{ cm}^{-2}$. The circles show the only threads in the image.

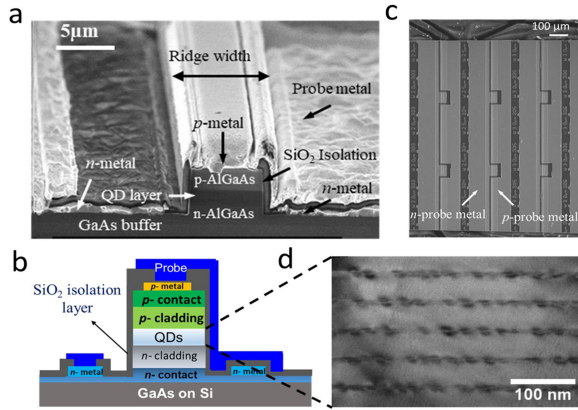


Fig. 3. (a) SEM image of the cross-section of an as-cleaved laser, tilted at 75° . (b) Schematic image of the laser cross-section, revealing the geometry of the contact and probe metals. (c) Top-down view of the laser bar. Each tick mark on the metal pad indicates a length of $100 \mu\text{m}$. (d) Bright-field TEM image of the active region cross-section, showing the five layers of QDs.

The dots were grown in an $\text{In}_{0.15}\text{Ga}_{0.85}\text{As}$ well with 2 nm below and 5 nm capping the dots followed by a 2.5 nm GaAs layer. The “In-flush” technique was employed at 580°C to improve dot uniformity [30]. The bottom cladding layers were grown at 580°C while the growth temperature for the top cladding layers was lowered to 560°C to reduce the QD intermixing. All temperatures were measured by pyrometer. The inset of Fig. 1(a) is the AFM image of the as grown dots, showing that the areal density of the dots is about $6.4 \times 10^{10} \text{ cm}^{-2}$.

Fig. 3 summarizes the structure of the as-fabricated laser devices. Fig. 3(a) and (b) show the SEM and schematic image of the laser cross-section, respectively. The laser ridges were formed perpendicular to the V-grooves by inductively coupled plasma (ICP) etching down to the n -contact layer. Laser facets were formed by cleaving, with cavity lengths of 750, 1450, and $2000 \mu\text{m}$ and ridge widths ranging from 1 to $10 \mu\text{m}$. Fig. 3(c) shows the top-down view of the as-cleaved laser bars. Sidewall scattering and surface recombination can be significant problems for the deeply etched devices. Thus, after ridge mesa formation, 12 nm of Al_2O_3 was applied by atomic-layer deposition (ALD) to passivate the side wall. An 800 nm thick SiO_2 layer was then deposited by sputtering for electrical isolation and to isolate the optical modes from the Pd/Ti/Pd/Au (p) and Pd/Ge/Pd/Au (n) metal contact layers. The five layers of QDs are clearly visible in the cross-section bright-field TEM image in Fig. 3(d), taken

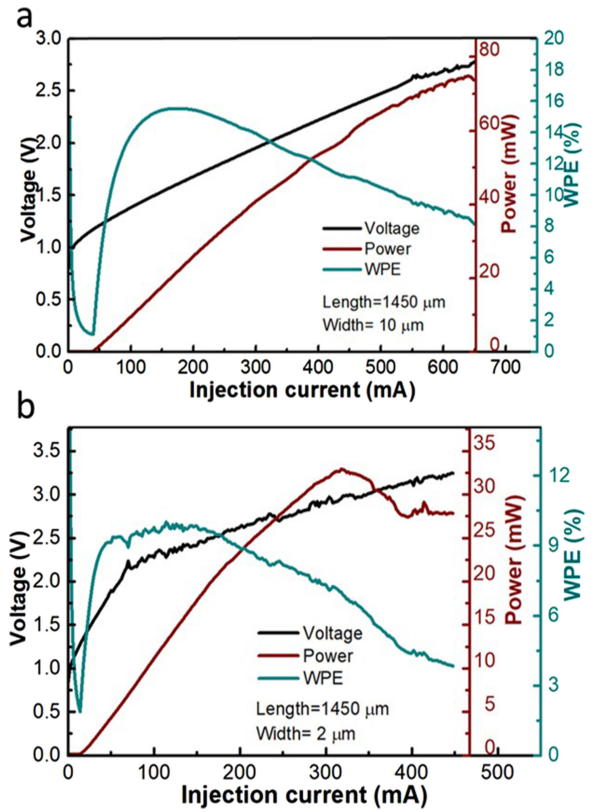


Fig. 4. Typical L-I-V characteristics of an as-cleaved laser with a cavity length of $1450 \mu\text{m}$ and a ridge width of (a) $10 \mu\text{m}$ and (b) $2 \mu\text{m}$, together with the wall-plug efficiency.

with $g = (002)$ under two beam condition. The individual dots revealed themselves as dark spots in the TEM image as they distort the surrounding lattice locally.

III. RESULTS AND DISCUSSION

110 ridge lasers were tested at room temperature under CW operation. Fig. 4(a) shows the typical light–current–voltage (LIV) characteristics of a laser with a $1450 \mu\text{m}$ cavity length and $10 \mu\text{m}$ ridge width. The measured 1 V turn-on voltage and 2.7Ω differential series resistance from the I-V curve indicate good metal contacts for efficient current injection. A clear knee behavior in the LI curve is observed at the lasing threshold current of 39 mA. This corresponds to a threshold current density (J_{th}) of 270 A/cm^2 , or 54 A/cm^2 per QD layer. No output saturation was observed when the output power reached 75 mW per facet at an injection current of 600 mA, which corresponds to a total output power exceeding 150 mW assuming equal output from both facets. Power roll over occurs until the injection reaches 650 mA. A maximum wall-plug efficiency of 15.6% was achieved. As a comparison, in Fig. 4(b), for a laser with the same cavity length of $1450 \mu\text{m}$, but a smaller ridge width of $2 \mu\text{m}$, the maximum power of 33 mW per facet is obtained at an injection current of 318 mA, with a threshold current of 16 mA.

Fig. 5 depicts a threshold current density histogram for all measured lasers, with the peak located around 400 to 500 A/cm^2 and a minimum of 270 A/cm^2 . As a comparison, our previously

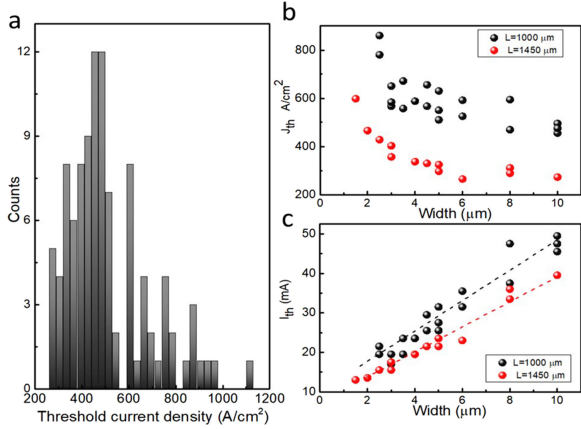


Fig. 5. Threshold current density distribution histogram for all measured lasers. Most of the devices fall between 300 and 500 A/cm². The inset shows a continuous decrease of threshold current with reduced ridge width, indicating good suppression of side-wall recombination.

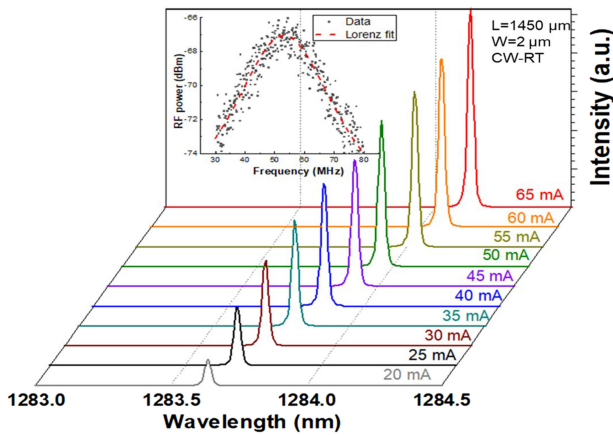


Fig. 6. Lasing spectra of a device with $2 \times 1450 \mu$ m² cavity. The primary lasing peak is located around 1284 nm. Single-mode operation was observed below 35 mA bias current. Inset: measured laser linewidth using self-heterodyne method.

reported lasers on the V-groove Si template had a threshold current density distribution peaked around 700 to 1000 A/cm². The main difference between the two is the threading dislocation density at the surface of the buffer. The inset of Fig. 5 shows a continuously decreasing trend of threshold current as the ridge width narrows down to 1.5 μ m. This suggests that the side wall recombination is greatly suppressed by the well-optimized Al₂O₃ passivation layer as well as the reduced carrier diffusion length from the QD active region. The higher threshold current with shorter cavities is due to the increase in the mirror loss. The typical carrier diffusion length of a QW active region is about 3 to 5 μ m, and this value is reduced to about 1 μ m with the QD active region [31]. The reduced carrier diffusion length is the reason for QD's insensitivity to internal defects as well as device side walls.

The spectra of a device with 1450 μ m cavity length and 2 μ m ridge width are shown in Fig. 6. The primary lasing peaking is located around 1284 nm. A slight red-shift of the lasing wavelength with increasing injection current was observed. It was interesting to notice that at low injection levels, namely less

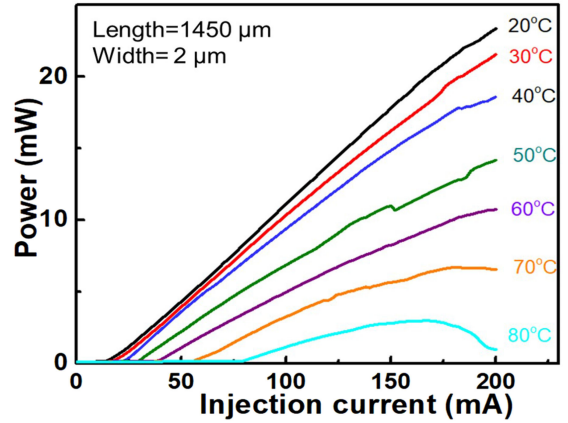


Fig. 7. High temperature measurements of the same device show lasing up to 80 $^{\circ}$ C under CW operation.

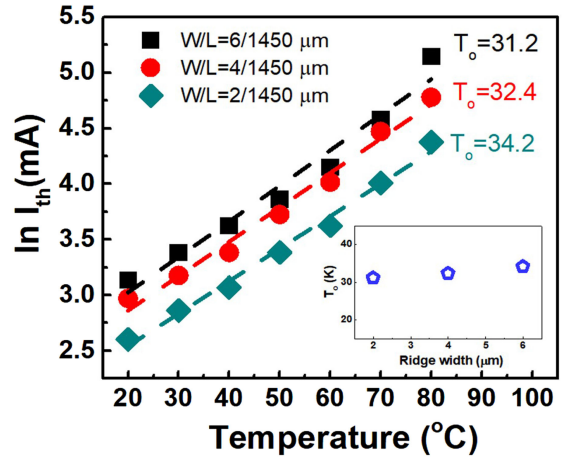


Fig. 8. Natural logarithm of threshold current versus stage temperature for ridge lasers with various width and a constant length of 1450 μ m. The dashed lines represent linear fitting to the experimental data. Inset: the corresponding characteristic temperature as a function of the ridge width, which shows narrowing of the laser ridge does not increase the temperature sensitivity of the threshold current.

than 35 mA, an apparent single mode operation was obtained with side-mode-suppression ratio of about 35 dB. There was a crack perpendicular to the ridge direction, suggesting that the realization of single-mode operation is due to the laser effectively operating as a coupled-cavity device with large cavity length ratio [32]. The inset of Fig. 6 shows the measured laser linewidth is about 14 MHz using self-heterodyne method.

We also tested the same device at elevated temperatures as shown in Fig. 7. The laser was able to function under CW operation up to 80 $^{\circ}$ C for ground state lasing, still producing an output power of ~ 4 mW. This demonstrates that the QD lasers on the V-groove Si template can meet the temperature requirement in a realistic datacenter environment. This result compares favorably to the best heterogeneously integrated quantum dot lasers on Si which operate CW up to 100 $^{\circ}$ C [33].

The natural logarithm of threshold current versus stage temperature for the ridge laser in Fig. 7 and other lasers with the same length but different widths are plotted in Fig. 8. Using an exponential function of $P_{th} \propto \exp(\frac{T}{T_0})$, the characteristic

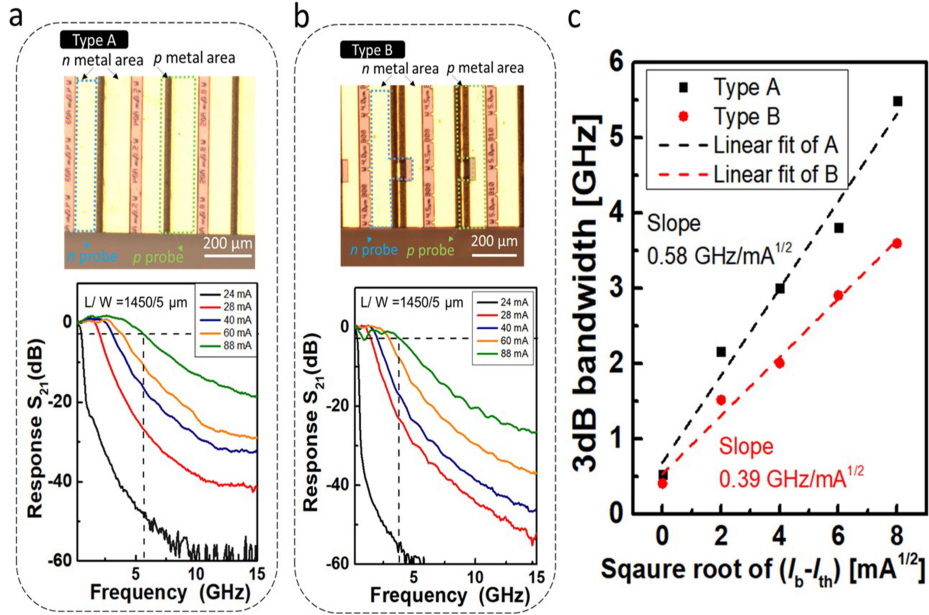


Fig. 9. Frequency response of (a) type A laser and (b) type B laser with the same dimension (length of $1450\ \mu\text{m}$ and a width of $5\ \mu\text{m}$) biased from 24 to 88 mA. The maximum $f_{3\text{dB}}$ saturated at 5.8 GHz for type A laser and 3.6 GHz for type B laser. The upper inset shows the microscopic image of the corresponding laser. (c) 3 dB bandwidth versus square root of the bias current above threshold of the two types of laser in (a) and (b). The dashed lines represent linear fitting to the experimental data.

temperature T_0 was extracted to fall into the range of 30–35 K, as shown in the inset of Fig. 8. Even though lasers with narrower ridges have smaller heat extraction area through the bottom Si to the heat sink, they are as insensitive, if not more, to temperature change as the lasers with wider ridges. There are two possible reasons. Firstly, a considerable amount of heat was extracted from the side walls, where narrower lasers had advantages with their higher area to volume ratio. Secondly, the residual thermal stress in GaAs on Si ($\sim 250\ \text{MPa}$) could be relieved with the higher aspect-ratio laser structures [34]. Fig. 9 depicts the small-signal modulation response, S_{21} , of type A laser and type B laser with the same dimension (length of $1450\ \mu\text{m}$ and a width of $5\ \mu\text{m}$) biased from 24 to 88 mA, respectively. For the type A laser in Fig. 9(a), the probe metals were designed in a way that there was no vertical overlap between the p - and n -contact metal due to the cross-over of p n probe metal. This is contrary to that of the type B laser in Fig. 9(b), where a portion of p -probe was placed upon the n -metal area with an 800 nm SiO_2 separation layer. Otherwise, the two structures are nominally the same in terms of epi structure and device fabrication. The 3 dB bandwidth, $f_{3\text{dB}}$, increased with increasing bias current and saturated at 5.8 GHz for type A laser and 3.6 GHz for type B laser when biased at 88 mA. The measurement procedure was similar to that described in [35]. The inset in Fig. 9 shows the plots of $f_{3\text{dB}}$ as a function of square root of bias current above threshold. The modulation efficiencies of $f_{3\text{dB}}$ for type A laser and type B laser are $0.58\ \text{GHz}/\text{mA}^{1/2}$ and $0.39\ \text{GHz}/\text{mA}^{1/2}$. The reduced parasitic capacitance of type A laser gives rise to a decent $f_{3\text{dB}}$ similar to that measured from the state-of-art result ($6.5\ \text{GHz}$ $f_{3\text{dB}}$ and $0.58\ \text{GHz}/\text{mA}^{1/2}$ modulation efficiency) on GaP/Si where 8 pairs of $\text{SiO}_2/\text{Ta}_2\text{O}_5$ films are coated on one facet to achieve a low mirror loss (99% reflection) and allow for lasing in small cavities (cavity length of $580\ \mu\text{m}$ and ridge

width of $3\ \mu\text{m}$) [35]. Note that the device presented here has a much longer length of $1450\ \mu\text{m}$ and a width of $5\ \mu\text{m}$, with both facets formed as cleaved. As a comparison, the recent reported maximum 3dB bandwidths and modulation current efficiency of QD laser grown on Si with as-cleaved facet is only 1.6 GHz and $0.4\ \text{GHz}/\text{mA}^{1/2}$ (cavity length of $2500\ \mu\text{m}$ and ridge width of $2.2\ \mu\text{m}$) [36]. With an optimized QD laser design readily based on the current growth process by scaling the number of QD layers and the cavity length, their modelling suggests that theoretical modulation bandwidth is only 5 GHz [27].

IV. CONCLUSION

In conclusion, we report a significant improvement of QD laser performance grown on V-grooved Si. The utilization of $\text{In}_{0.1}\text{Ga}_{0.9}\text{As}$ strained layers and cycles of temperature annealing reduces the TDD from 7×10^7 to $3 \times 10^6\ \text{cm}^{-2}$. This translates into a reduced minimum threshold current density from $\sim 700\ \text{A}/\text{cm}^2$ to $\sim 286\ \text{A}/\text{cm}^2$, with minimum threshold current of 12 mA and a maximum operating temperature of $80\ ^\circ\text{C}$. By optimizing the probe design, a maximum 3 dB bandwidth of 5.8 GHz has been achieved, which exceeds the previous theoretical prediction of modulation bandwidth [27]. Commercial use will require stable long-term operation above room temperature without an additional active cooling system. It has been reported that the main cause of device failure during prolonged operation is the growth of dislocation networks in the laser material [37]. Despite the QD's insensitivity to defects, the in-plane misfit dislocations interacting with multiple QDs in a row can be detrimental to device performance. Such misfit dislocations are thought to nucleate from existing TDs. Since reducing the number of TDs can effectively increase the energy barrier to nucleate misfit dislocations [38], lasers

grown on GaAs-on-Si buffer with lower TDD are expected to possess higher reliability during device operation. According to the investigation of the impact of threading dislocation density on the reliability [39], reducing the dislocation density from 2.8×10^8 to $7.3 \times 10^6 \text{ cm}^{-2}$ has improved the laser lifetime from a few thousand hours to more than $10 \times 10^6 \text{ h}$ at $35 \text{ }^\circ\text{C}$ and at twice the threshold current density. With the record low TDD ($3 \times 10^6 \text{ cm}^{-2}$) buffer on patterned Si, one can envision further improved lifetime.

ACKNOWLEDGMENT

The authors would like to thank UCSB nanofabrication clean room staff for helpful discussions and assistance.

REFERENCES

- [1] Cisco Visual Networking, "The zettabyte era—Trends and analysis," Cisco, San Jose, CA, USA, White Paper, 2017.
- [2] J. Gaudette, "Workshop at executive forum 208," Microsoft, Redmond, WA, USA, 2018.
- [3] J. E. Bowers and A. Y. Liu, "A comparison of four approaches to photonic integration," in *Proc. Opt. Fiber Commun. Conf. Exhib.*, Mar. 2017, Paper M2B-4.
- [4] T. Komljenovic *et al.*, "Photonics integrated circuits using heterogeneous integration on silicon," *Proc. IEEE*, vol. 106, no. 12, pp. 2246–2257, Dec. 2018.
- [5] K. Nishi, K. Takemasa, M. Sugawara, and Y. Arakawa, "Development of quantum dot lasers for data-com and silicon photonics applications," *IEEE J. Sel. Topics Quantum Electron.*, vol. 23, no. 6, Nov./Dec. 2017, Art. no. 1901007.
- [6] D. Bimberg and U. W. Pohl, "Quantum dots: Promises and accomplishments," *Mater. Today*, vol. 14, no. 9, pp. 388–397, 2011.
- [7] Z. I. Kazi, T. Egawa, T. Jimbo, and M. Umeno, "First room-temperature continuous-wave operation of self-formed InGaAs quantum dot-like laser on Si substrate grown by metalorganic chemical vapor deposition," *Jpn. J. Appl. Phys.*, vol. 39, no. 7R, 2000, Art. no. 3860.
- [8] S. Chen *et al.*, "Electrically pumped continuous-wave III–V quantum dot lasers on silicon," *Nature Photon.*, vol. 10, pp. 307–311, 2016.
- [9] Y. Wang *et al.*, "Electrically-pumped continuous-wave quantum-dot distributed feedback laser array on silicon," *Optica*, vol. 5, no. 5, pp. 528–533, 2018.
- [10] J. C. Norman, D. Jung, Y. Wan, and J. E. Bowers, "Perspective: The future of quantum dot photonic integrated circuits," *APL Photon.*, vol. 3, no. 3, 2018, Art. no. 030901.
- [11] D. Jung *et al.*, "High efficiency low threshold current $1.3 \mu\text{m}$ InAs quantum dot lasers on on-axis (001) GaP/Si," *Appl. Phys. Lett.*, vol. 111, no. 12, 2017, Art. no. 122107.
- [12] Y. Wan *et al.*, " $1.3 \mu\text{m}$ submilliwatt threshold quantum dot micro-lasers on Si," *Optica*, vol. 4, no. 8, pp. 940–944, Aug. 2017.
- [13] S. Liu *et al.*, "High-channel-count low-noise 20 GHz passively mode locked quantum dot laser directly grown on Si with 4.1 Tbit/s transmission capacity," *Optica*, vol. 6, no. 2, pp. 128–134, 2019.
- [14] R. W. Herrick *et al.*, "Reliability of quantum well and quantum dot lasers for silicon photonics (invited)," in *Proc. IEEE Photon. Conf.*, 2017, p. 11.
- [15] D. Jung *et al.*, "Highly reliable low threshold InAs quantum dot lasers on on-axis (001) Si with 87% injection efficiency," *ACS Photon.*, vol. 5, no. 3, pp. 1094–1100, 2018.
- [16] Z. I. Kazi, P. Thilakan, T. Egawa, M. Umeno, and T. Jimbo, "Realization of GaAs/AlGaAs lasers on Si using epitaxial lateral overgrowth by metalorganic chemical vapor deposition," *Jpn. J. Appl. Phys.*, vol. 40, pp. 4903–4906, 2001.
- [17] K. Li *et al.*, "O-band InAs/GaAs quantum dot laser monolithically integrated on exact (001) Si substrate," *J. Crystal Growth*, vol. 511, pp. 56–60, 2019.
- [18] Y. Wang *et al.*, "Three-step growth of metamorphic GaAs on Si (001) by low-pressure metal organic chemical vapor deposition," *J. Vacuum Sci. Technol. B, Nanotechnol. Microelectron.: Mater., Process., Meas., Phenomena*, vol. 31, no. 5, 2013, Art. no. 051211.
- [19] J. Kwoen *et al.*, "All MBE grown InAs/GaAs quantum dot lasers on on-axis Si (001)," *Opt. Express*, vol. 26, no. 9, pp. 11568–11576, 2018.
- [20] R. Alcotte *et al.*, "Epitaxial growth of antiphase boundary free GaAs layer on 300 mm Si (001) substrate by metalorganic chemical vapour deposition with high mobility," *APL Mater.*, vol. 4, no. 4, 2016, Art. no. 046101.
- [21] W.-Q. Wei *et al.*, "InAs QDs on (111)-faceted Si (001) hollow substrates with strong emission at 1300 nm and 1550 nm," *Appl. Phys. Lett.*, vol. 113, no. 5, 2018, Art. no. 053107.
- [22] Y. Wan *et al.*, "Optically pumped $1.3 \mu\text{m}$ room-temperature InAs quantum dot micro-disk lasers directly grown on (001) silicon," *Opt. Lett.*, vol. 41, pp. 1664–1667, 2016.
- [23] J. Norman *et al.*, "Electrically pumped continuous wave quantum dot lasers epitaxially grown on patterned, on-axis (001) Si," *Opt. Exp.*, vol. 25, no. 4, pp. 3927–3934, 2017.
- [24] Q. Li, K. W. Ng, and K. M. Lau, "Growing antiphase-domain-free GaAs thin films out of highly ordered planar nanowire arrays on exact (001) silicon," *Appl. Phys. Lett.*, vol. 106, 2015, Art. no. 072105.
- [25] Y. Wan *et al.*, "O-band electrically injected quantum dot micro-ring lasers on on-axis (001) GaP/Si and V-groove Si," *Opt. Express*, vol. 25, pp. 26853–26860, 2017.
- [26] Y. Wan *et al.*, "Sub-wavelength InAs quantum dot micro-disk lasers epitaxially grown on exact Si (001) substrates," *Appl. Phys. Lett.*, vol. 108, 2016, Art. no. 221101.
- [27] C. Hantschmann *et al.*, "Small-signal modulation and analysis of monolithic $1.3 \mu\text{m}$ InAs/GaAs quantum dot lasers on silicon," in *Proc. Eur. Conf. Opt. Commun.*, 2018, pp. 1–3.
- [28] K. Bernardette *et al.*, "How to control defect formation in monolithic III/V hetero-epitaxy on (100) Si? A critical review on current approaches," *Semicond. Sci. Technol.*, vol. 33, no. 9, 2018, Art. no. 093002.
- [29] S. Yuting *et al.*, "Optical pumped InGaAs/GaAs nano-ridge laser epitaxially grown on a standard 300-mm Si wafer," *Optica*, vol. 4, no. 12, pp. 1468–1473, 2017.
- [30] S. Haffouz *et al.*, "Growth and fabrication of quantum dots superluminescent diodes using the indium-flush technique: A new approach in controlling the bandwidth," *J. Crystal Growth*, vol. 311, pp. 1803–1806, 2009.
- [31] S. A. Moore *et al.*, "Reduced surface sidewall recombination and diffusion in quantum-dot lasers," *IEEE Photon. Technol. Lett.*, vol. 18, no. 17, pp. 1861–1863, Sep. 2006.
- [32] J. Bowers *et al.*, "Cleaved-coupled-cavity lasers with large cavity length ratios for enhanced stability," *Appl. Phys. Lett.*, vol. 44, pp. 821–823, 1984.
- [33] G. Kurczveil, D. Liang, M. Fiorentino, and R. G. Beausoleil, "Robust hybrid quantum dot laser for integrated silicon photonics," *Opt. Express*, vol. 24, no. 14, pp. 16167–16174, 2016.
- [34] A. Vega-Flick, D. Jung, S. Yue, J. E. Bowers, and B. Liao, "Reduced thermal conductivity of epitaxial GaAs on Si due to symmetry-breaking biaxial strain," *Phys. Rev. Mater.*, vol. 3, 2019, Art. no. 034603.
- [35] D. Inoue *et al.*, "Directly modulated $13 \mu\text{m}$ quantum dot lasers epitaxially grown on silicon," *Opt. Express*, vol. 26, no. 6, pp. 7022–7033, 2018.
- [36] C. Hantschmann *et al.*, "Understanding the bandwidth limitations in monolithic $1.3 \mu\text{m}$ InAs/GaAs quantum dot lasers on silicon," *J. Lightw. Technol.*, vol. 37, no. 3, pp. 949–955, Feb. 2019.
- [37] J. Van der Ziel, R. Dupuis, R. Logan, and C. Pinzone, "Degradation of GaAs lasers grown by metalorganic chemical vapor deposition on Si substrates," *Appl. Phys. Lett.*, vol. 51, no. 2, pp. 89–91, 1987.
- [38] A. Y. Liu *et al.*, "Reliability of InAs/GaAs quantum dot lasers epitaxially grown on silicon," *IEEE J. Sel. Topics Quantum Electron.*, vol. 21, no. 6, Nov./Dec. 2015, Art. no. 1900708.
- [39] D. Jung *et al.*, "Impact of threading dislocation density on the lifetime of InAs quantum dot lasers on Si," *Appl. Phys. Lett.*, vol. 112, no. 15, 2018, Art. no. 153507.



Chen Shang received the B.S. degree in material science and engineering from Purdue University, West Lafayette, IN, USA, in 2016. He is currently working toward the Ph.D. degree in materials with the University of California, Santa Barbara, Santa Barbara, CA, USA.

His research interests include InAs quantum dots on InP lattice constant for telecom application and low defect density III–V buffer structure grown on Si via molecular beam epitaxy. He is a recipient of the Peter J. Frenkel Foundation Fellowship.



Yating Wan received the Ph.D. degree from the Department of Electrical and Computer Engineering, The Hong Kong University of Science and Technology, Hong Kong, in 2017. In 2017, she joined Prof. J. Bower's group with the University of California, Santa Barbara, as a Postdoctoral Research Associate. Her research interests include microcavity quantum dot optoelectronics and silicon photonics. She was the recipient of the Ph.D. Research Excellence Award in 2016–2017.



Justin C. Norman (S'14–M'18) received the B.S. degrees in chemical engineering and physics from the University of Arkansas at Fayetteville, Fayetteville, AR, USA, in 2013, and the Ph.D. degree in materials from the University of California, Santa Barbara, Santa Barbara, CA, USA, in 2018.

He is currently a Postdoctoral Researcher with the University of California. His research interests are in the growth of InAs quantum dots via molecular beam epitaxy for applications in photonics and quantum electrodynamics. He also works on the heteroepitaxy

of III–V materials on Si for photonic integration. He was the National Science Foundation Graduate Research Fellow and a Frenkel Foundation Fellow in the University of California.



Noelle Collins is currently working toward the Ph.D. degree with the University of California, Santa Barbara, Santa Barbara, CA, USA. Her research interests include characterization and modeling of quantum dot laser epitaxially grown on silicon as well as passive–active integration of photonic devices with quantum dot active region on monolithic III–V on silicon platform.



Ian MacFarlane is currently working as a Research Intern with the University of California, Santa Barbara, Santa Barbara, CA, USA. His research interests include characterization of quantum dot laser epitaxially grown on silicon as well as passive–active integration of photonic devices with quantum dot active region on monolithic III–V on silicon platform.

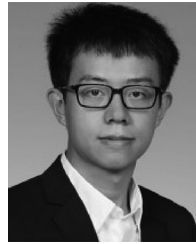


Mario Dumont is currently working toward the Ph.D. degree with the University of California, Santa Barbara, Santa Barbara, CA, USA. His research interests include characterization and modeling of quantum dot laser epitaxially grown on silicon as well as passive–active integration of photonic devices with quantum dot active region on monolithic III–V on silicon platform.



Songtao Liu received the B.E. (Hons.) degree in electronic information science and technology from Henan University, Kaifeng, China, in 2012, and the Ph.D. degree in microelectronics and solid state electronics in 2017 from the University of Chinese Academy of Sciences, Beijing, China, where his Ph.D. dissertation was on monolithically integrated InP-based mode-locked lasers.

He is currently a Postdoctoral Researcher with the University of California, Santa Barbara, Santa Barbara, CA, USA. His research interests are in the field of photonic integrated circuits, with an emphasis on monolithically integrated mode-locked lasers and tunable lasers both on InP and silicon platforms.

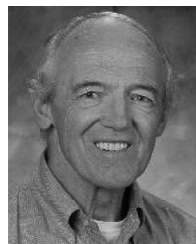


Qiang Li (S'12–M'15) received the B.S. degree from Peking University, Beijing, China, in 2009, and the Ph.D. degree from The Hong Kong University of Science and Technology, Hong Kong, in 2014. He is currently a Lecturer with the School of Physics and Astronomy, Cardiff University, Cardiff, U.K. His current research interests include epitaxial integration of III–V high mobility transistors and lasers on silicon substrate by metal–organic chemical vapor deposition.



Kei M. Lau (S'78–M'80–SM'92–F'01) received the B.S. and M.S. degrees in physics from the University of Minnesota, Minneapolis, MN, USA, in 1976 and 1977, respectively, and the Ph.D. degree in electrical engineering from Rice University, Houston, TX, USA, in 1981. She is currently a Chair Professor with the Department of Electronic and Computer Engineering, The Hong Kong University of Science and Technology (HKUST), Hong Kong. She was on the faculty with the Department of Electrical and Computer Engineering, University of

Massachusetts/Amherst before joining HKUST in 2000. Her group's research interests are primarily III–V and wide bandgap semiconductor materials and devices, for integration on silicon.



Arthur C. Gossard (SM'88–F'01–LF'12) was born in Ottawa, IL, USA, in 1935. He received the B.A. (*summa cum laude*) degree in physics from Harvard University, Cambridge, MA, USA, in 1956, and the Ph.D. degree in physics from the University of California, Berkeley, Berkeley, CA, USA, in 1960.

He was a member of Technical Staff with AT&T Bell Telephone Laboratories from 1960 to 1987. He then became a Professor with the University of California, Santa Barbara, Santa Barbara, CA, USA, where he has been serving since 1987. His current

research interests center on molecular beam epitaxial crystal growth and on the creation and application of artificially structured quantum materials.

Prof. Gossard is a member of the American Physical Society and the Materials Research Society. He discovered the first nuclear magnetic resonance in ferromagnets. He also grew the first alternate monolayer superlattices and created the first high mobility modulation doped semiconductors. He co-discovered fractional quantization of the quantum Hall effect and the quantum confined Stark effect. He is a Member of both the National Academy of Sciences and the National Academy of Engineering.



John E. Bowers received the M.S. and Ph.D. degrees from Stanford University, Stanford, CA, USA. He was with the AT&T Bell Laboratories. He is currently a Director of the Institute for Energy Efficiency and a Professor with the Departments of Electrical and Computer Engineering and Materials, University of California, Santa Barbara, Santa Barbara, CA, USA. His research interests are primarily concerned with silicon photonics, optoelectronic devices, optical switching and transparent optical networks, and quantum dot lasers. He is a Fellow of the OSA and

the American Physical Society, and a recipient of the IEEE Photonics Award, OSA/IEEE Tyndall Award, the IEEE LEOS William Streifer Award, and the South Coast Business and Technology Entrepreneur of the Year Award. He is a Member of the National Academy of Engineering and the National Academy of Inventors.